Photolysis of 4-Oxo-2-pentenal in the 190−460 nm Region

Bin Xiang, Lei Zhu,* and Yongxin Tang†

Wadsworth Center, New York State Department of Health, and Department of Environmental Health Sciences, State University of New York, Albany, New York 12201-0509

Received: May 23, 2007; In Final Form: July 18, 2007

We have studied the gas-phase photolysis of 4-oxo-2-pentenal by laser photolysis combined with cavity ring-down spectroscopy. Absorption cross sections of *cis*- and *trans*-4-oxo-2-pentenal have been measured in the 190−460 nm region. The product channel following 193, 248, 308, and 351 nm photolysis of 4-oxo-2-pentenal was investigated. The HCO radical is a photodissociation product of 4-oxo-2-pentenal only at 193 and 248 nm. The HCO quantum yields from the photolysis of a mainly *trans*-4-oxo-2-pentenal sample are 0.13 ± 0.02 and 0.014 ± 0.003 at 193 and 248 nm, where errors quoted (1σ) represent experimental scatter. The HCO quantum yields from the photolysis of a mainly *cis*-4-oxo-2-pentenal sample are 0.078 ± 0.012 and 0.018 ± 0.007 at 193 and 248 nm, where errors quoted (1σ) represent experimental scatter. The end-products from 193, 248, 308, and 351 nm photolysis of 4-oxo-2-pentenal (the 4-oxo-2-pentenal sample had a tran/cis ratio of 1.062:1) have been determined by FTIR. Ethane, methyl vinyl ketone, and 5-methyl-3*H*-furan-2-one have been observed, suggesting the occurrence of 4-oxo-2-pentenal photolysis pathways such as $CH_3COCH{=}CHCHO + h\nu \rightarrow CH_3 + COCH{=}CHCHO$, $CH_3COCH{=}CHCHO + h\nu \rightarrow CH_3COCH{=}CH_2 + CO$, and $CH_3COCH{=}CHCHO + h\nu \rightarrow$ 5-methyl-3*H*-furan-2-one. The estimated yields for the $CH_3 + COCH{=}CHCHO$ channel are about 25%, 33%, 31%, and 23% at 193, 248, 308, and 351 nm, respectively. The absolute uncertainties in the determination of $CH_3 + COCH{=}CHCHO$ yields are within 55% at 193 nm, and 65% at 248, 308, and 351 nm. The estimated yields for the $CH_3COCH{=}CH_2 + CO$ channel are about 25%, 23%, 40%, and 33% at 193, 248, 308, and 351 nm, respectively. The absolute uncertainties in the determination of $CH_3COCH{=}CH_2$ yields are within 80% at 193 and 248 nm and 65% at 308 and 351 nm. The estimated yields for the 5-methyl-3*H*-furan-2-one channel are about 1.2%, 2.1%, 5.3%, and 5.5% at 193, 248, 308, and 351 nm, respectively. The absolute uncertainties in the determination of 5-methyl-3*H*-furan-2-one yields are about 23%, 86%, 40%, and 46% at 193, 248, 308, and 351 nm. Results from our investigation indicate that photolysis is a dominant removal pathway for 4-oxo-2-pentenal degradation in the atmosphere.

1. Introduction

4-Oxo-2-pentenal ($CH_3C(O)CH{=}CHC(O)H$) is an unsaturated dicarbonyl. It has been identified as a product formed from photochemical oxidation of toluene, *m*-xylene, and 2-methylfuran.[1−8] Photolysis and reactions with OH, O_3, and NO_3 are its possible gas-phase removal pathways in the atmosphere. The rate constant for reaction of *trans-/cis*-4-oxo-2-pentenal with OH has been measured by using the relative rate technique, and was found to be 5.6×10^{-11} cm^3 molecule^{-1} s^{-1} at 296 K.[9] Bierbach et al.[9] studied the photolysis of 4-oxo-2-pentenal in air and concluded that photolysis is probably a stronger sink for 4-oxo-2-pentenal than is the OH radical reaction. When a visible lamp (320 nm $\leq \lambda \leq$ 480 nm; $\lambda_{max} = 360$ nm) was used to irradiate a mixture of the cis/trans isomers of 4-oxo-2-pentenal in air, the major products observed were maleic anhydride, 5-methyl-3*H*-furan-2-one, HCHO, CH_3OH, and CH_3OOH, along with 20−30% trans/cis isomerization product. When a UV lamp ($\lambda = 254$ nm) was used to irradiate a *cis*- and *trans*-4-oxo-2-pentenal mixture in air, the major products observed were maleic anhydride, HCHO, CH_3OH, and CH_3OOH; the minor products were 5-methyl-3*H*-furan-2-one and ethyne, along with ≤20% trans/cis isomerization product. Irradiation of 4-oxo-2-pentenal in air with a UV lamp resulted in a significant increase in the yield of maleic anhydride, a corresponding increase in the yields of HCHO, CH_3OH, and CH_3OOH, and a corresponding decrease in 5-methyl-3*H*-furan-2-one formation, relative to the yields obtained with the visible lamp. However, the impurities in the samples of Bierbach et al. prevented those authors from determining the initial concentration of 4-oxo-2-pentenal, and from quantifying the photolysis quantum yield of 4-oxo-2-pentenal. With an improved synthetic method, Liu et al.[10,11] were able to produce 4-oxo-2-pentenal with purity ≥90%. They studied OH- and O_3-initiated photooxidation of 4-oxo-2-pentenal in a smog chamber, and obtained an O_3/4-oxo-2-pentenal reaction rate constant of 4.8×10^{-18} cm^3 molecule^{-1} s^{-1} at 293−297 K. Although Liu et al. were unable to detect maleic anhydride resulting from the photolysis of 4-oxo-2-pentenal, they did detect a very small amount of methyl vinyl ketone. They also measured the solution-phase UV/visible absorption spectrum of 4-oxo-2-pentenal in the 290−500 nm region.[11] However, the gas-phase UV/visible

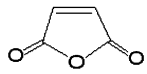

maleic anhydride

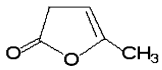

5-methyl-3H-furan-2-one

* Address correspondence to this author. Phone: 518-474-6846. Fax: 518-473-2895. E-mail: zhul@wadsworth.org.

† Current address: Atmospheric Chemistry Division, National Center for Atmospheric Research, Boulder, CO 80307.

10.1021/jp0739972 CCC: $37.00
Published on Web 08/24/2007

absorption spectrum of 4-oxo-2-pentenal has not been previously reported. Determination of the UV/visible absorption cross sections, photolysis product channels, and quantum yields of gaseous 4-oxo-2-pentenal as a function of wavelength is necessary, in order to elucidate the atmospheric fates of aromatic hydrocarbons. This information is also needed in the atmospheric chemistry model that simulates photochemical degradation of aromatic hydrocarbons.[12]

Photolysis of 4-oxo-2-pentenal can occur through the following pathways:

$$\textit{trans-/cis}\text{-}CH_3COCH{=}CHCHO + h\nu$$

$$\rightarrow \textit{cis-/trans}\text{-}CH_3COCH{=}CHCHO \quad (1)$$

$$\rightarrow \text{5-methyl-3}\textit{H}\text{-furan-2-one} \quad (2)$$

$$\rightarrow CH_3 + COCH{=}CHCHO \quad (3)$$

$$\rightarrow CH_3CO + CH{=}CHCHO \quad (4)$$

$$\rightarrow CH_3COCH{=}CH + HCO \quad (5)$$

$$\rightarrow CH_3COCH{=}CH_2 + CO \quad (6)$$

Pathway 1 is a trans/cis photoisomerization channel. Pathway 2 is a photoinduced intramolecular rearrangement channel that involves a 1,2-H-shift. Pathways 3−5 are radical formation channels. Pathway 6 is a molecular elimination channel. To form HCO + $CH_3COCH{=}CH$ and CH_3CO + CH=CHCHO from the photolysis of 4-oxo-2-pentenal, C−C bonds in the conjugated π-system ($O{=}C(CH_3){-}CH{=}CH{-}C(H){=}O$) must be broken. The photochemical thresholds for these channels are expected to be at wavelengths shorter than those of ∼346 nm for the formation of R + HCO and R + R′C(O) from the photolysis of saturated aliphatic aldehydes (RCHO) and ketones (RCOR′). The threshold wavelength for the formation of CH_3 + COCH=CHCHO is expected to be equal to or longer than the threshold wavelength (∼351 nm) for the formation of CH_3 + CH_3CO from the photolysis of acetone. In this paper, we report results obtained from the gas-phase photolysis of 4-oxo-2-pentenal by the methodology of laser photolysis combined with cavity ring-down spectroscopy.[13,14] Absorption cross sections of *cis*- and *trans*-4-oxo-2-pentenal in the 190−460 nm region have been obtained. We have probed for the HCO product following 193, 248, 308, and 351 nm photolysis of 4-oxo-2-pentenal. The HCO radical was only observed at 193 and 248 nm; the corresponding HCO quantum yields from the photolysis of a mainly *cis*-4-oxo-2-pentenal sample and a mainly *trans*-4-oxo-2-pentenal sample have been measured. The end-products from the photolysis of 4-oxo-2-pentenal at 193, 248, 308, and 351 nm have been determined by using FTIR, and their yields have been estimated.

2. Experimental Technique

Detailed descriptions of our experimental setup can be found elsewhere.[15−17] An excimer laser, operating at 193, 248, 308, and 351 nm, was used to photolyze 4-oxo-2-pentenal. Cavity ring-down spectroscopy was used to probe the HCO radical product. The probe laser source for the cavity ring-down spectrometer was a nitrogen-pumped dye laser system. The reaction cell was vacuum-sealed with a pair of highly reflective cavity mirrors. The output from the excimer laser was introduced into the reaction cell at a 15° angle to the main optical axis of the cell, through a sidearm. The probe laser beam was directed along the main optical axis of the cell, and its path overlapped with that of the photolysis beam at the center of the reaction cell. A fraction of the probe laser beam was transmitted into the cavity through the front mirror; the photon intensity decay inside the cavity was monitored via measurement of the weak transmission of light through the rear mirror with a photomultiplier tube (PMT). The PMT output was amplified, digitized, and sent to a computer. The decay curve was fitted to a single-exponential decay function, from which the ring-down time constant (τ) and the total loss (Γ) per optical pass were calculated. By measuring the cavity losses with and without a photolysis pulse, we obtained the HCO absorption due to the photolysis of 4-oxo-2-pentenal. A pulse/delay generator was used to vary the delay time between the firings of the photolysis and probe lasers. 4-Oxo-2-pentenal pressure between 0.02 and 1.1 Torr was used in the measurement of the HCO quantum yield. Quantum yield measurements were obtained at a laser repetition rate of 0.1 Hz. The spectrum scan was carried out at a laser repetition rate of 1 Hz. Absorption cross sections of 4-oxo-2-pentenal in the 280−460 nm region were determined by feeding either the fundamental or the second harmonic output of an excimer-pumped dye laser directly into the ring-down cavity (but at a much reduced fluence level), and then monitoring changes in cavity losses in the presence of varying concentrations of 4-oxo-2-pentenal. Absorbance of the probe beam by 4-oxo-2-pentenal at a given pressure can be obtained by measuring the cavity losses with and without 4-oxo-2-pentenal in the cell. The absorption cross section of 4-oxo-2-pentenal at a given wavelength was extracted from the slope of a plot of absorbance versus 4-oxo-2-pentenal concentration in the cell. Since the probe laser beam was reflected back and forth between the center of the front cavity mirror and the center of the back cavity mirror, the absorbing path length was fixed in the cavity ring-down cross section measurement; it was equal to the distance between two cavity mirrors (50 cm). Gas pressure was measured at the center of the reaction cell by an MKS 622A Baratran capacitance manometer (1 Torr maximum pressure, measurement accuracy is ≤0.25% of the pressure reading). As can be seen from the NMR spectrum described in the Results section, our synthesized 4-oxo-2-pentenal sample was essentially free of detectable impurities. Pure samples of 4-oxo-2-pentenal in the 0.006−0.109 Torr pressure range were used for cross section measurements in the 280−460 nm region. Laser dyes used to cover the 280−460 nm region include coumarin 153, rhodamin 6G, rhodamin B, rhodamin 101, DCM, PTP, BBQ, DPS, stilbene, and C120. An FTIR (IFS 66v; Bruker Optics) was used to measure the infrared absorption spectra of 4-oxo-2-pentenal and its photolysis end-products. All experiments were carried out at an ambient temperature of 295 ± 2 K.

4-Oxo-2-pentenal was prepared by using a synthetic procedure modified from the literature.[18] A solution of 11.2 mL of bromine (0.22 mol) in 60 mL of methanol was added dropwise to a mixture containing 2-methylfuran (18 mL, 0.2 mol), anhydrous Na_2CO_3 (42.4 g, 0.4 mol), and methanol (100 mL) at −10 °C over a time period of 1 h. The reaction mixture was stirred at −10 °C for 3 h, and the undissolved salts were removed by filtration. The filtrate was poured into 400 mL of saturated NaCl solution, extracted with CH_2Cl_2 (4 × 60 mL), and dried over anhydrous Na_2SO_4. After removal of CH_2Cl_2, the resulting yellow oil was added to 60 mL of distilled water and stirred for 1 day, followed by extraction with CH_2Cl_2 (4 × 15 mL). The CH_2Cl_2 extracts were dried over Na_2SO_4 and distilled at 65−70 °C under vacuum (11 Torr). The collected yellow oil was a mixture of *cis*- and *trans*-4-oxo-2-pentenal; the samples produced had trans/cis ratios of 1:0.128, 1.062:1, and 0.082:1. (Although we followed the same synthetic procedure each time,

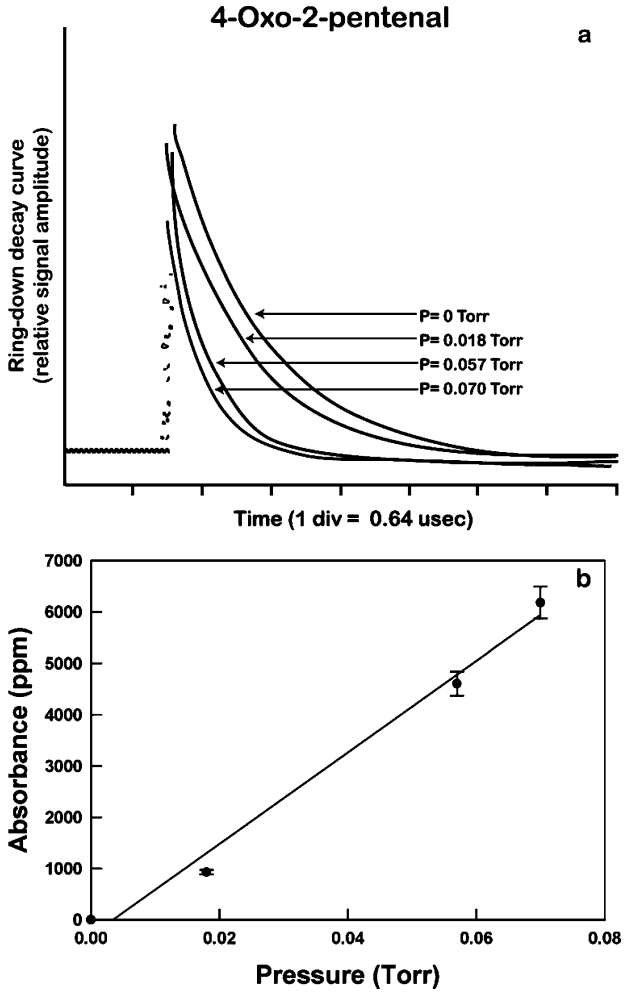

Figure 1. (a) Ring-down decay curves at 300 nm with an evacuated cavity, or with 0.018, 0.057, and 0.070 Torr of 4-oxo-2-pentenal in the cavity; this 4-oxo-2-pentenal sample had a trans/cis ratio of 1:0.128. (b) Absorbances (base e) plotted against 4-oxo-2-pentenal pressure in the cavity.

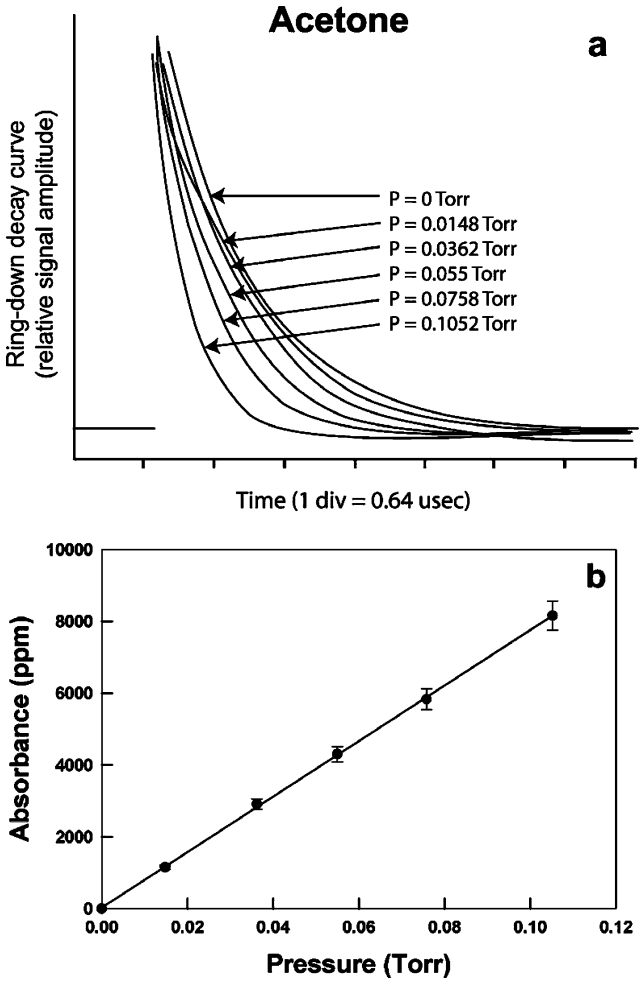

Figure 2. (a) Ring-down decay curves at 300 nm with an empty cavity, or with 0.0148, 0.0362, 0.0550, 0.0758, and 0.1052 Torr of acetone inside the cavity. (b) Absorbances (base e) plotted against acetone pressure in the cavity.

we were not able to control the ratio of cis- and trans-isomer generated from 4-oxo-2-pentenal synthesis) Before each experiment, the sample was further purified by repeated freeze−pump−thaw cycles at −78 °C. The room temperature vapor pressure of *cis-/trans*-4-oxo-2-pentenal is about 1.2 Torr. Formaldehyde was generated by pyrolysis of paraformaldehyde (≥95% purity; Aldrich) at 110 °C. CCl_4 (≥99.9% purity; Aldrich) was purified by repeated freeze−pump−thaw cycles. Nitrogen (≥99.999% purity; BOC Edwards) was used without further purification.

3. Results and Discussion

3.1. Absorption Cross Sections of 4-Oxo-2-pentenal in the 190−460 nm Region. We have determined the gas-phase UV/visible absorption cross sections of 4-oxo-2-pentenal in the 190−460 nm region, at 295 ± 2 K. The absorption cross sections of 4-oxo-2-pentenal in the 280−460 nm region were measured directly by cavity ring-down spectroscopy. The absorption cross sections of 4-oxo-2-pentenal at 193 and 248 nm were obtained by measurement of the transmitted photolysis photon intensity as a function of 4-oxo-2-pentenal pressure in the cell, followed by application of Beer's law to the experimental data. The absorption cross sections of 4-oxo-2-pentenal in the 190−250 nm region were determined by addition of various amounts of 4-oxo-2-pentenal in a 10 cm long quartz cell, insertion of the cell into the beam path of a Beckman DU640 UV Spectrometer outside of our lab, and then determination of the UV absorption spectra of 4-oxo-2-pentenal as a function of its pressure in the cell. We did not use single-path absorption by 4-oxo-2-pentenal in a 10 cm long cell to extract absorption cross sections of 4-oxo-2-pentenal at wavelengths longer than 250 nm because the UV/visible absorption of 4-oxo-2-pentenal is much smaller at wavelengths longer than 250 nm than at wavelengths in the 190−250 nm region. For cavity ring-down cross section measurements, pure 4-oxo-2-pentenal sample was used under static conditions; the residence time of the 4-oxo-2-pentenal sample inside the cavity was about 1 min for a given 4-oxo-2-pentenal pressure. Shown in Figure 1a as an example are ring-down decay curves at 300 nm with an evacuated cavity, and with 0.018, 0.057, and 0.070 Torr of a mainly *trans*-4-oxo-2-pentenal sample in the cavity. The ring-down laser pulse energy was about 0.78 μJ/pulse at 300 nm. The round-trip cavity losses corresponding to the decay curves shown in Figure 1a are 4021, 4950, 8627, and 10201 ppm, respectively. Absorbances of the 300 nm radiation by 4-oxo-2-pentenal at 0.018, 0.057, and 0.070 Torr pressures are 929, 4606, and 6180 ppm, respectively. By plotting absorbance against 4-oxo-2-pentenal pressure in the cavity (shown in Figure 1b), we can extract the absorption cross section of 4-oxo-2-pentenal at 300 nm from the slope of the plot (slope = 89281 ppm/Torr). The 4-oxo-2-pentenal absorption cross section thus obtained is 2.72×10^{-20} cm^2/molecule at 300 nm, for the mainly *trans*-4-oxo-2-pentenal sample. To verify

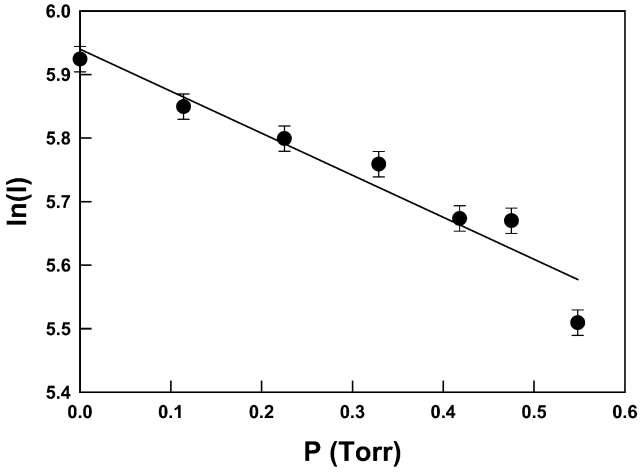

Figure 3. Semilog plot of the transmitted 248 nm photolysis fluence as a function of 4-oxo-2-pentenal pressure inside the cell. The 4-oxo-2-pentenal sample used here had a trans/cis ratio of 1:0.128. Circles are experimental data. The solid line is a fit to the data with intercept, slope, and r^2 values of 5.940, −0.661, and 0.924, respectively.

the suitability of using the cavity ring-down method to measure UV absorption cross sections of carbonyl species, we added a carbonyl compound (e.g., acetone) into the cavity, and compared the cross section value that we obtained with the known gas-phase absorption cross section of the compound at 300 nm. Shown in Figure 2a are ring-down decay curves at 300 nm with an empty cavity, and with 0.0148, 0.0362, 0.0550, 0.0758, and 0.1052 Torr of acetone inside the cavity. The round-trip cavity losses that correspond to these decay curves are 4075, 5224, 6989, 8377, 9906, and 12232 ppm, respectively. Absorbances of the 300 nm radiation by acetone at 0.0148, 0.0362, 0.0550, 0.0758, and 0.1052 Torr pressures are 1149, 2914, 4302, 5831, and 8157 ppm, respectively. By plotting absorbances against acetone pressure in the cavity (shown in Figure 2b), we extracted the absorption cross section of acetone at 300 nm from the slope of the plot (slope = 77234 ppm/Torr). The absorption cross section of acetone thus obtained is 2.38×10^{-20} cm^2/molecule at 300 nm. The recommended[19] absorption cross section value of acetone at 300 nm is 2.77×10^{-20} cm^2/molecule at 298 K. The gas-phase acetone cross section value that we obtained at 300 nm agrees within 14% with the recommended acetone cross section value at this wavelength. Thus, the cavity ring-down method is shown to be suitable for measurement of carbonyl species absorption cross sections in the UV region. Figure 3 shows a semilog plot of the transmitted 248 nm photolysis fluence, measured at the end of the cell's sidearm as a function of 4-oxo-2-pentenal pressure inside the cell, for a mainly *trans*-4-oxo-2-pentenal sample. The 4-oxo-2-pentenal absorption cross section of 4.79×10^{-19} cm^2/molecule at 248 nm was derived from the slope of the plot (0.661/Torr) and the length of the cell's sidearm (42.1 cm). Cross section values for 4-oxo-2-pentenal determined in this study by using various methods are plotted in Figure 4a. As can be seen from the figure, the gas-phase UV/visible absorption spectrum of 4-oxo-2-pentenal is composed of an absorption band in the shorter wavelength region ($\pi \rightarrow \pi^*$ transition) and broad absorption bands in the longer wavelength region (most likely composed of two partially overlapping n $\rightarrow \pi^*$ transitions); the shorter wavelength band is about 2 orders of magnitude stronger than the bands in the longer wavelength region. The two n$\rightarrow\pi^*$ bands for a saturated dialdehyde, such as methylglyoxal,[20−22] peak at 290 and 430 nm. There is some similarity between the gas-phase UV/visible absorption spectrum of 4-oxo-2-pentenal obtained from the current study and the previously reported[23,24] gas-phase UV/visible absorption spectra of *E*,*E*-2,4-hexadienal ($CH_3CH{=}CH{-}$

TABLE 1: Absorption Cross Sections of *cis*-/*trans*-4-Oxo-2-pentenal (in Units of cm^2 molecule^{-1}) as a Function of Wavelength

λ (nm)	$10^{20}\sigma$	λ (nm)	$10^{20}\sigma$	λ (nm)	$10^{20}\sigma$	λ (nm)	$10^{20}\sigma_{cis}$	$10^{20}\sigma_{trans}$
190	274[a]	211	351	232	150	193	849 ± 46[b,c]	444 ± 46
191	309	212	354	233	137	248	66.2 ± 5.0[b,c]	37.8 ± 9.1
192	247	213	355	234	124	280	3.72 ± 0.36[b,d]	1.39 ± 0.12
193	243	214	357	235	112	290	1.33 ± 0.04	2.09 ± 0.35
194	315	215	358	236	99.4	300	1.18 ± 0.28	2.74 ± 0.48
195	357	216	356	237	88.7	310	1.51 ± 0.22	4.76 ± 0.38
196	257	217	352	238	79.5	320	2.37 ± 0.18	2.42 ± 0.07
197	208	218	344	239	70.8	330	3.99 ± 0.37	4.37 ± 0.32
198	212	219	337	240	63.0	340	4.36 ± 0.44	4.63 ± 0.31
199	224	220	327	241	56.9	350	5.08 ± 0.30	3.69 ± 0.20
200	237	221	317	242	52.1	360	4.47 ± 0.23	3.69 ± 0.29
201	249	222	307	243	48.2	370	4.07 ± 0.62	2.67 ± 0.44
202	262	223	295	244	45.1	380	2.47 ± 0.57	3.26 ± 0.34
203	275	224	281	245	61.2	390	2.53 ± 0.53	2.54 ± 0.25
204	291	225	264	246	40.5	400	2.22 ± 0.27	1.94 ± 0.22
205	304	226	246	247	39.3	410	1.82 ± 0.09	0.75 ± 0.09
206	313	227	226	248	38.0	420	1.22 ± 0.18	0.59 ± 0.08
207	323	228	210	249	36.8	430	1.14 ± 0.12	0.29 ± 0.03
208	331	229	194	250	55.6	440	0.73 ± 0.07	0.29 ± 0.05
209	340	230	179			450	0.60 ± 0.01	0.13 ± 0.01
210	347	231	165			460	0.38 ± 0.05	0.11 ± 0.05

[a] Cross section data at 1 nm intervals in the 190−250 nm region. Cross sections were determined by insertion of a 10 cm long cell into the beam path of a UV/visible spectrometer, with variation of the 4-oxo-2-pentenal pressure in the cell and monitoring of the corresponding changes in the absorbance of the UV/visible beam; the 4-oxo-2-pentenal sample had a trans/cis ratio of 0.082:1. The absolute uncertainty in these cross section data is about 40−70%. [b] Errors quoted represent measurement precision. [c] Cross section data at 193 and 248 nm were determined by monitoring transmitted photolysis fluence as a function of 4-oxo-2-pentenal pressure in the cell. The overall uncertainties in the determination of *cis*-4-oxo-2-pentenal cross sections are 10% at 193 and 248 nm. The overall uncertainties in the determination of *trans*-4-oxo-2-pentenal cross sections are 15% at 193 nm and 25% at 248 nm. [d] Cross section data at 10 nm intervals in the 280−460 nm region determined by cavity ring-down spectroscopy. The overall uncertainties in the determination of *cis*-4-oxo-2-pentenal cross sections are within 5% at 290 and 450 nm, 10% at 320, 350, 360, and 410 nm, 15% at 280, 330, 340, 400, 430, 440, and 460 nm, 20% at 310, 370, and 420 nm, 25% at 380 and 390 nm, and 30% at 300 nm. The overall uncertainties in the determination of *trans*-4-oxo-2-pentenal cross sections are within 5% at 320 nm, 10% at 310 and 450 nm and the 330−360 nm region, 15% at 280 and 430 nm and in the 380−410 nm region, 20% at 290, 300, 370, 420, and 440 nm, and 50% at 460 nm.

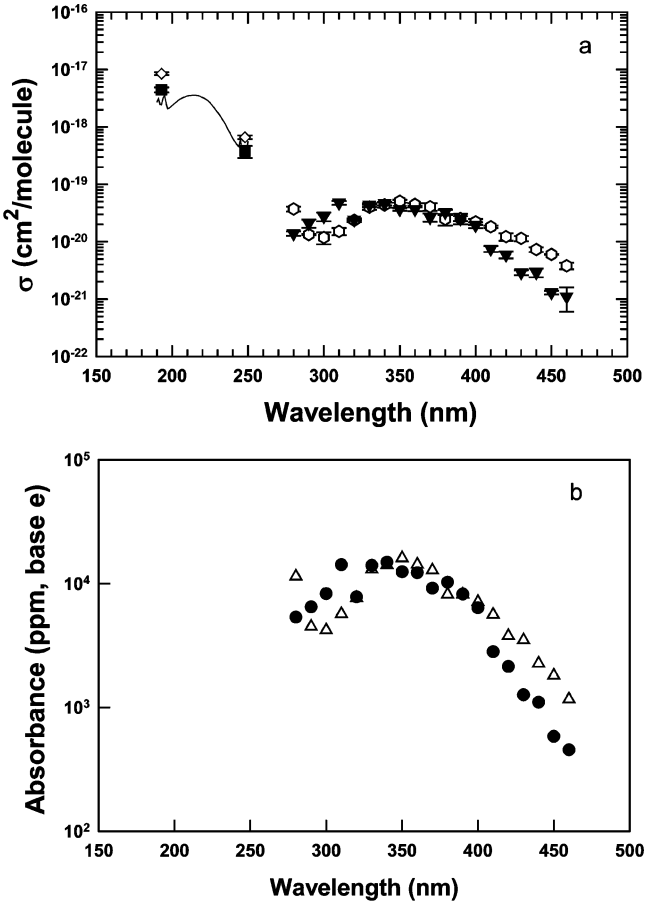

Figure 4. (a) Absorption cross sections for 4-oxo-2-pentenal (σ) as a function of wavelength. Hexagons: Cross sections in the 280−460 nm region determined by using cavity ring-down spectroscopy and extracted for *cis*-4-oxo-2-pentenal. Triangles down: Cross sections in the 280−460 nm region determined by using cavity ring-down spectroscopy and extracted for *trans*-4-oxo-2-pentenal. Solid line: Cross sections determined by insertion of a 10 cm long cell into the beam path of a UV/visible spectrometer, with variation of the 4-oxo-2-pentenal pressure in the cell and monitoring of the corresponding changes in the absorbance of the UV/visible beam; the 4-oxo-2-pentenal sample had a trans/cis ratio of 0.082:1. Squares: Cross sections determined by monitoring transmitted photolysis fluence as a function of 4-oxo-2-pentenal pressure in the cell and extracted for *trans*-4-oxo-2-pentenal. Diamonds: Cross sections determined by monitoring transmitted photolysis fluence as a function of 4-oxo-2-pentenal pressure in the cell and extracted for *cis*-4-oxo-2-pentenal. (b) Round-trip UV absorbances in the 280−460 nm region determined by using cavity ring-down spectroscopy. Triangles up represent absorbances for the 4-oxo-2-pentenal sample that had a trans/cis ratio of 0.082:1. Circles represent absorbances for the 4-oxo-2-pentenal sample that had a trans/cis ratio of 1:0.128. The pressure of 4-oxo-2-pentenal in the ring-down cavity was 0.1 Torr.

CH═CHCHO) and butenedial (HCOCH═CHCHO). Figure 4b shows that there is some difference in the UV/visible absorbances obtained with use of 4-oxo-2-pentenal sample made mainly of cis-isomer and 4-oxo-2-pentenal sample made mainly of trans-isomer. Since we have measured 4-oxo-2-pentenal cross section data using samples consisting mainly of cis-isomer and samples consisting mainly of trans-isomer, we can de-convolute isomer-specific cross section data based upon the percentage of cis- and trans-isomer in the particular cis/trans mixture; the isomer-specific cross section values for 4-oxo-2-pentenal thus extracted are plotted in Figure 4a and listed in Table 1. The errors quoted (1σ) represent the estimated precision of cross section determination calculated from error propagation involved

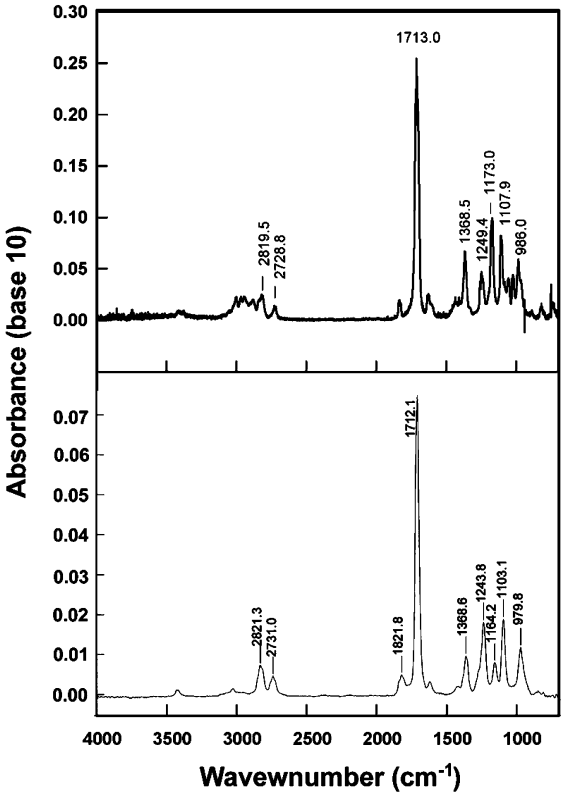

Figure 5. Infrared spectrum of the 4-oxo-2-pentenal vapor in the 700−4000 cm^{-1} region. Upper panel: IR absorption spectrum (acquired at 0.5 cm^{-1} resolution) determined in this work; the 4-oxo-2-pentenal sample had a trans/cis ratio of 1.062:1; a sample pressure of 0.027 Torr was used. Lower panel: IR absorption spectrum reported by Smith et al.[4]

in the determination of the cross sections for mainly cis- and mainly trans-isomers. Considering both random errors and systematic errors, the overall uncertainties in the determination of *cis*-4-oxo-2-pentenal cross sections are within 5% at 290 and 450 nm, 10% at 193, 248, 320, 350, 360, and 410 nm, 15% at 280, 330, 340, 400, 430, 440, and 460 nm, 20% at 310, 370, and 420 nm, 25% at 380 and 390 nm, and 30% at 300 nm. The overall uncertainties in the determination of *trans*-4-oxo-2-pentenal cross sections are within 5% at 320 nm, 10% at 310 and 450 nm and in the 330−360 nm region, 15% at 193, 280, and 430 nm and in the 380−410 nm region, 20% at 290, 300, 370, 420, and 440 nm, 25% at 248 nm, and 50% at 460 nm.

3.2. FTIR and NMR Spectra of 4-Oxo-2-pentenal. We measured infrared absorption spectra of 4-oxo-2-pentenal vapor in the 700−4000 cm^{-1} region. Shown in Figure 5 is an IR absorption spectrum of 4-oxo-2-pentenal, for a 4-oxo-2-pentenal sample having a trans/cis ratio of 1.062:1, along with an IR spectrum of 4-oxo-2-pentenal reported by Smith et al.[4] Our 4-oxo-2-pentenal IR spectrum was acquired at room temperature and at 0.5 cm^{-1} resolution, while that obtained by Smith et al.[4] was acquired at 8 cm^{-1} resolution and with a lightpipe accessory operated at 250 °C. As seen from the figure, the IR spectrum of 4-oxo-2-pentenal obtained by our group and that obtained by Smith et al. appear similar; the major peak position agrees well between the two studies, and the minor peak positions differ by not more than 9 cm^{-1}; these small-scale differences are possibly due to the different spectral resolutions used in acquiring the spectra, as well as the different operating temperatures, which can alter the ratio of cis- and trans-isomers. The infrared absorption spectra of 4-oxo-2-pentenal in the 800−2000 and 2600−3100 cm^{-1} regions were also reported previ-

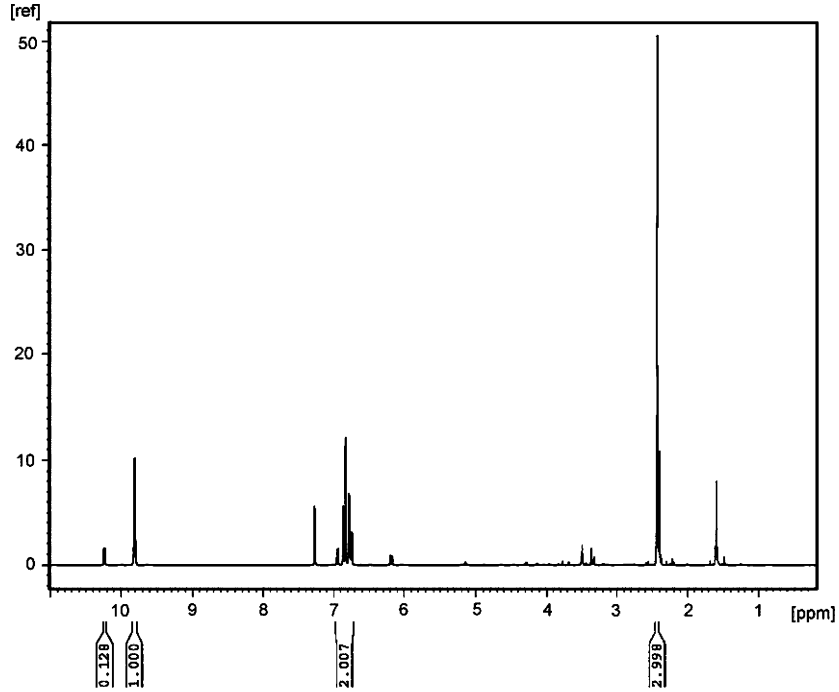

Figure 6. ^{1}H NMR spectrum of 4-oxo-2-pentenal synthesized in this work. This 4-oxo-2-pentenal sample has a trans/cis ratio of 1:0.128.

ously by Bierbach et al.[9] Our 4-oxo-2-pentenal IR spectrum shows reasonable agreement with those obtained by Bierbach et al.,[9] in terms of IR peak positions. The IR spectra obtained by Bierbach et al.[9] were corrected for known impurities in their systems and had a low signal-to-noise ratio. Since there are a lot of overlapping peaks between the cis- and trans-isomers of 4-oxo-2-pentenal in the IR spectrum, it was not possible to distinguish cis-isomer from trans-isomer by using the IR spectrum.

We also measured the NMR spectrum of 4-oxo-2-pentenal. Shown in Figure 6 is an NMR spectrum of one of our synthesized 4-oxo-2-pentenal samples, displaying the following ^{1}H NMR ($CDCl_3$) peaks: 2.427 (s, 3H, CH_3), 6.739, 6.753, 6.771, 6.785, 6.832, 6.865, 6.935, 6.958 (m, 2H, CH═CH), 9.801, 9.815, 10.226, 10.240 (two d, 1H, CHO). The NMR analysis indicated that this 4-oxo-2-pentenal sample had a trans/cis ratio of 1.000:0.128.

3.3. Time-Resolved Studies of the Photolysis of 4-Oxo-2-pentenal at 193, 248, 308, and 351 nm. *3.3.1. General Features.* We investigated the photolysis of 4-oxo-2-pentenal at 193, 248, 308, and 351 nm, but we only found the HCO radical in the 193 and 248 nm photolysis of 4-oxo-2-pentenal. The lack of HCO product from the photolysis of 4-oxo-2-pentenal at 308 and 351 nm suggests that the photolysis of unsaturated dialdehyde is very different from the photolysis of a saturated dialdehyde such as methylglyoxal (CH_3COCHO). Our group previously[22] determined the HCO quantum yields from the photolysis of methylglyoxal in the 290−440 nm region; the reported HCO quantum yields were 0.9 ± 0.1 at 308 nm and 1.1 ± 0.2 at 351 nm. For HCO + CH_3COCH═CH to be formed from the photolysis of 4-oxo-2-pentenal, a C−C bond in the conjugated π system (O═C−C═C−C═O) must be broken. The lack of HCO product from the photolysis of 4-oxo-2-pentenal at 308 and 351 nm is most likely the result of the higher photon energy required to break a C−C bond in the conjugated π system. A less likely possibility is that the HCO signal size from the 308 and 351 nm photolysis of 4-oxo-2-pentenal is below the HCO detection limit. Upper limits for the HCO quantum yields from the photolysis of 4-oxo-2-pentenal are <0.1% at 308 and 351 nm photolysis wavelengths.

3.3.2. HCO Radical Quantum Yields from the Photolysis of 4-Oxo-2-pentenal at 193 and 248 nm. The cavity ring-down absorption spectrum of the product after 193 and 248 nm photolysis of a mainly *trans*-4-oxo-2-pentenal sample is similar to the previously reported[15,16,22,24,25] absorption spectrum of HCO in the 613−617 nm region, suggesting that the HCO radical is a photolysis product of 4-oxo-2-pentenal at these two wavelengths. The cavity ring-down spectrometer was tuned to the HCO X^2A'' (0,0,0) → A^2A' (0,9,0) R bandhead at 613.8 nm, and the HCO absorption resulting from the photolysis of 4-oxo-2-pentenal was determined. The HCO quantum yield from the photolysis of 4-oxo-2-pentenal was determined from the ratio of the HCO concentration produced in the pump/probe laser overlap region to the absorbed photon density in the same region. The overlap region can be conceptualized as a rectangular solid with its center overlapping that of the cell, with its width and height defined by dimensions of the photolysis beam, and with the length of the rectangular solid defined by (beam width) × $(\tan 15°)^{-1}$, where 15° is the crossing angle between the pump and the probe laser beams. The length of the photolysis/probe laser overlap region is defined by (beam width) × $(\sin 15°)^{-1}$. The absorbed photolysis photon density in the pump/probe laser overlap region can be derived from the difference between the transmitted photolysis beam energies entering (E_{in}) and leaving (E_{out}) the overlap region, the individual photon energy (hc/λ) at the photolysis wavelength (λ), and the volume (v) of the overlap region by the formula

$$\text{absorbed photon density} = \frac{E_{in} - E_{out}}{h\frac{c}{\lambda}v}$$

The photolysis beam energy entering or leaving the pump/probe laser overlap region can be calculated from the incident photolysis beam energy entering the cell (E_0), the absorption cross section (σ), the density (n) of 4-oxo-2-pentenal in the cell, and the absorbing path length by application of Beer's law:

$$E_{in} = E_0 \exp(-\sigma n l_1)$$

$$E_{out} = E_0 \exp(-\sigma n l_2)$$

where l_1 is the distance between the photolysis beam entrance and the beginning of the pump/probe laser overlap region, and l_2 is the distance between the photolysis beam entrance and the end of the pump/probe laser overlap region. The incident photolysis beam energy (E_0) was measured by a calibrated Joulemeter placed in front of the cell. After the photolysis beam passed through the front cell window, it experienced transmission loss. The window transmission loss was determined by measuring photolysis fluence both before the cell and after an empty cell. The incident beam energy inside the cell was corrected for photolysis beam transmission loss at the front cell window, and for reflection of the photolysis beam from the rear cell window. The HCO concentration following 4-oxo-2-pentenal photolysis was obtained by measurement of HCO's absorption at 613.80 nm at a photolysis laser and a probe laser delay of 15 μs. The absolute HCO concentration from 193 nm photolysis of 4-oxo-2-pentenal was calibrated relative to the HCO concentration from the Cl + H_2CO → HCO + HCl reaction, with 193 nm photolysis of CCl_4 used as the Cl atom precursor. CCl_4 was first freeze−pump−thawed and then mixed with formaldehyde in a gas manifold. The calibrated CCl_4/H_2CO mixture ($P_{CCl_4}/P_{H_2CO} = 1/10$) was transferred into a gas bulb before it was introduced into the reaction cell. Partial pressures of CCl_4 and H_2CO inside the cell were calculated from their total pressure in the cell and their percentages in the mixture. The HCO concentration from 248 nm photolysis of 4-oxo-2-pentenal was calibrated relative to formaldehyde photolysis at 248 nm, for which a recommended HCO quantum yield value ($\varphi = 0.29$) is available.[19] The HCO absorption cross section at 613.80 nm obtained from 193 and 248 nm calibration experiments agreed within 25% with our previously reported[16] HCO absorption cross section of $\sim 2.0 \times 10^{-18}$ cm^2/molecule at this wavelength. The dependence of the HCO quantum yields on nitrogen buffer gas pressure (0.3−49.7 Torr) was examined; no dependence was observed. The HCO quantum yield showed a weak increase with increasing 4-oxo-2-pentenal pressure but it still fell within the range of the scatter of the experimental data. The average HCO quantum yield from the 193 nm photolysis of 0.05−0.5 Torr of a mainly *trans*-4-oxo-2-pentenal sample was 0.13 ± 0.02. The average HCO quantum yield from the 248 nm photolysis of 0.1−1.1 Torr of a mainly *trans*-4-oxo-2-pentenal sample was 0.014 ± 0.003. The errors quoted (1σ) are the estimated precision of quantum yield determinations. Systematic errors in the determination of HCO quantum yield include uncertainties in the determination of the following: HCO absorption cross section (∼25%), 4-oxo-2-pentenal concentration and absorption cross section (∼10% at 193 nm and ∼22% at 248 nm), pulse energy (∼5%), and angle between photolysis and probe lasers (3%). With both random and systematic errors taken into account, the overall uncertainty in the determination of HCO quantum yields is about 58% at 193 nm, and about 76% at 248 nm. We also photolyzed a sample of 4-oxo-2-pentenal composed mainly of cis-isomer. Pressures of 4-oxo-2-pentenal used were 0.026−0.15 Torr in the 193 nm photolysis experiments and 0.038−0.091 Torr in the 248 nm photolysis experiments. The average HCO quantum yields are 0.078 ± 0.012 at 193 nm and 0.018 ± 0.007 at 248 nm, where errors quoted (1σ) represent experimental scatter. The absolute uncertainty in the determination of HCO quantum yield from the photolysis of a mainly *cis*-4-oxo-2-pentenal sample is about 55% at 193 nm and about 81% at 248 nm.

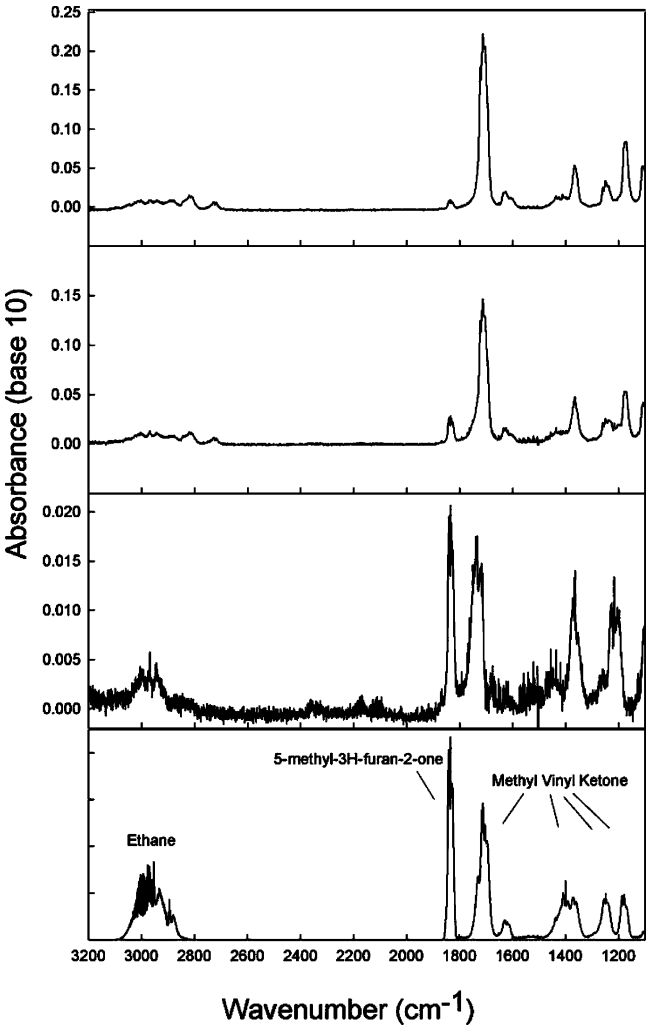

Figure 7. Shown from top to bottom: FTIR spectrum of 0.026 Torr of 4-oxo-2-pentenal without photolysis; FTIR spectrum after photolysis of 0.026 Torr of 4-oxo-2-pentenal at 351 nm; FTIR spectrum of the photolysis end-products after subtraction of unphotolyzed 4-oxo-2-pentenal; and FTIR spectrum for the sample standards of ethane, methyl vinyl ketone, and 5-methyl-3*H*-furan-2-one. The 4-oxo-2-pentenal sample had a trans/cis ratio of 1.062:1.

3.4. Photolysis End-Product Studies with FTIR at 193, 248, 308, and 351 nm. 4-Oxo-2-pentenal was photolyzed in a stainless steel White cell mounted on top of a Bruker IFS66v FTIR spectrometer. 4-Oxo-2-pentenal pressure of 0.026 Torr was used. The end-products from the 193, 248, 308, and 351 nm photolysis of a sample of 4-oxo-2-pentenal with a trans/cis ratio of 1.062:1 were analyzed by using FTIR. Presented in Figure 7 are IR spectra of 4-oxo-2-pentenal (0.5 cm^{-1} resolution) both without photolysis and with 351 nm photolysis; the spectrum of the photolysis end-products; and IR standard spectra for 5-methyl-3*H*-furan-2-one, ethane, and methyl vinyl ketone. The similarity between the photolysis end-product spectrum and the sample-standard spectra indicates that 5-methyl-3*H*-furan-2-one, ethane, and methyl vinyl ketone are end-products of the photolysis of 4-oxo-2-pentenal at 351 nm. 5-Methyl-3*H*-furan-2-one, ethane, and methyl vinyl ketone were also observed from the photolysis of 4-oxo-2-pentenal at 193, 248, and 308 nm. 5-Methyl-3*H*-furan-2-one is a product of the 4-oxo-2-pentenal photolysis channel:

$$\textit{trans-/cis-}CH_3COCH{=}CHCHO + h\nu \rightarrow \text{5-methyl-3}H\text{-furan-2-one} \quad (2)$$

Ethane is likely formed from the following 4-oxo-2-pentenal photolysis channel and the subsequent $CH_3 + CH_3$ reaction:

$$\textit{trans-/cis}\text{-}CH_3COCH{=}CHCHO + h\nu \rightarrow CH_3 + COCH{=}CHCHO \quad (3)$$

Methyl vinyl ketone is possibly a product of the 4-oxo-2-pentenal photolysis channel:

$$\textit{trans-/cis}\text{-}CH_3COCH{=}CHCHO + h\nu \rightarrow CH_3COCH{=}CH_2 + CO \quad (6)$$

In addition to the 5-methyl-3*H*-furan-2-one, ethane, and methyl vinyl ketone bands, an IR absorption band peaking at 3016 cm^{-1} was observed following the photolysis of 4-oxo-2-pentenal at 193 and 248 nm. This photolysis end-product was attributed to methane, and it is possibly a product of the following 4-oxo-2-pentenal photolysis channel:

$$\textit{trans-/cis}\text{-}CH_3COCH{=}CHCHO + h\nu \rightarrow CH_3CO + CH{=}CHCHO \quad (4)$$

The lifetimes of the CH_3CO radical following 193 nm photolysis of a number of ketones were measured previously.[26−28] Photolysis-generated CH_3CO has lifetimes ranging from 3.1 ps for acetone, 8.6 ps for $CH_3COC_2H_5$, 15 ps for $CH_3COC_3H_7$, to 23 ps for $CH_3COCH(CH_3)_2$. By analogy, the CH_3CO radical generated from 193 and 248 nm photolysis of 4-oxo-2-pentenal likely had lifetimes on the order of picoseconds, it underwent decomposition into CH_3 and CO, and the CH_3 radical thus formed further reacted to form methane. Significantly increased CO formation was also observed from the 193 and 248 nm photolysis of 4-oxo-2-pentenal.

By using the sample standards to calibrate the photolysis products' IR spectra, and by simultaneously measuring the amount of 4-oxo-2-pentenal photolyzed, we obtained estimated yields of the $CH_3COCH{=}CH_2 + CO$, $CH_3 + COCH{=}CHCHO$, and 5-methyl-3*H*-furan-2-one channels from the photolysis of 4-oxo-2-pentenal at 193, 248, 308, and 351 nm; these yield data are listed in Table 2. Estimated yields of $CH_3COCH{=}CH_2 + CO$ from the photolysis of 4-oxo-2-pentenal at 193, 248, 308, and 351 nm are 25%, 23%, 40%, and 33%, respectively. Estimated yields of $CH_3 + COCH{=}CHCHO$ from the photolysis of 4-oxo-2-pentenal at 193, 248, 308, and 351 nm are 25%, 33%, 31%, and 23%, respectively. Yields of 5-methyl-3*H*-furan-2-one from the 193, 248, 308, and 351 nm photolysis of 4-oxo-2-pentenal are approximately 1.2%, 2.1%, 5.3%, and 5.5%, respectively. The sum of the end-product yields from the photolysis of 4-oxo-2-pentenal at 193, 248, 308, and 351 nm is not unity possibly because the yield of the trans/cis isomerization channel was not included in the summation. Our measurements were not sensitive to the photoisomerization yields. Previous study by Bierbach et al.[9] indicated the trans/cis isomerization yield following the photolysis of a *cis-/trans*-4-oxo-2-pentenal mixture in air was about 20−30% with visible lamp irradiation ($320 \leq \lambda \leq 480$ nm) and ≤20% with UV lamp irradiation ($\lambda = 254$ nm). After adding the end-products yields determined from this study and the trans/cis isomerization yields determined by Bierbach et al., we found the total photolysis product yields of 4-oxo-2-pentenal to be close to unity. Thus, secondary losses of the end-products were not significant in our experiments. Liu et al.[10] detected a very small amount of methyl vinyl ketone when photolyzing 4-oxo-2-pentenal in a smog chamber, but they did not report its yield. Our current work tentatively confirms the occurrence of the methyl vinyl ketone channel from the photolysis of 4-oxo-2-pentenal; we also estimated the yield of this photolysis channel. Bierbach et al.[9] studied the photolysis of a mixture of the cis/trans isomers of 4-oxo-2-pentenal in air. The major products that they detected following visible lamp irradiation of 4-oxo-2-pentenal were maleic anhydride, 5-methyl-3*H*-furan-2-one, HCHO, CH_3OH, and CH_3OOH. When a UV lamp was used to irradiate the *cis*- and *trans*-4-oxo-2-pentenal mixture in air, the major products determined were maleic anhydride, HCHO, CH_3OH, and CH_3OOH; the minor products were 5-methyl-3*H*-furan-2-one and ethyne. Bierbach et al.'s finding of HCHO, CH_3OH, and CH_3OOH following the photolysis of 4-oxo-2-pentenal in air suggests that CH_3 is a photolysis product of 4-oxo-2-pentenal; the results of our present study are consistent with their observation. Since Bierbach et al.[9] were not able to obtain absolute photolysis product yields, a quantitative comparison of our results with theirs is not possible. We did not observe maleic anhydride as a photolysis product of 4-oxo-2-pentenal, since our end-product study was done in the absence of air. Maleic anhydride can be formed from the reaction of O_2 with $COCH{=}CHCHO$, a coproduct of the $CH_3 + COCH{=}CHCHO$ channel from the photolysis of 4-oxo-2-pentenal. Although we observed 5-methyl-3*H*-furan-2-one from the photolysis of 4-oxo-2-pentenal at 193, 248, 308, and 351 nm, that is a minor photolysis pathway compared with the $CH_3COCH{=}CH_2 + CO$ and $CH_3 + COCH{=}CHCHO$ channels. Bierbach et al.[9] indicated that the yield of 5-methyl-3*H*-furan-2-one is smaller with UV-lamp irradiation of 4-oxo-2-pentenal than with visible-lamp irradiation. Our finding in the present study, that the 5-methyl-3*H*-furan-2-one yield is lower at shorter photolysis wavelengths, is consistent with their observation. We did not find acetylene as a product of the photolysis of 4-oxo-2-pentenal at the photolysis wavelengths investigated.

3.5. Atmospheric Photolysis Rate Constants for 4-Oxo-2-pentenal. We have estimated the atmospheric photolysis rate constants ($k_{photolysis}$) of 4-oxo-2-pentenal using the relationship

$$k_{photolysis} = \sum \sigma(\lambda)\cdot\varphi(\lambda)\cdot J(\lambda)\Delta\lambda$$

where $J(\lambda)$ represents actinic solar flux, $\sigma(\lambda)$ represents the gas-phase absorption cross sections of *cis*- and *trans*-4-oxo-2-

TABLE 2: Product Yields[a,b] (%) from the Photolysis of 4-Oxo-2-pentenal

λ (nm)	$\varphi_{CH_3+COCH=CHCHO}$	$\varphi_{CH_3COCH=CH_2+CO}$	$\varphi_{5-methyl-3H-furan-2-one}$	φ_{CH_3CO}
193	25 ± 8	25 ± 10	1.2 ± 0.1	11 ± 3
248	33 ± 10	23 ± 8	2.1 ± 1.5	17 ± 9
308	31 ± 12	40 ± 10	5.3 ± 1.3	0
351	23 ± 9	33 ± 9	5.5 ± 1.7	0

[a] Errors quoted only represent relative measurement error. [b] The absolute uncertainties in the determination of 5-methyl-3*H*-furan-2-one yields are about 23%, 86%, 40%, and 46% at 193, 248, 308, and 351 nm. The absolute uncertainties in the determination of $CH_3 + COCH{=}CHCHO$ yields are within 55% at 193 nm and 65% at 248, 308, and 351 nm. The absolute uncertainties in the determination of CH_3CO yields are about 57% at 193 nm and 83% at 248 nm. The absolute uncertainties in the determination of $CH_3COCH{=}CH_2$ yields are within 80% at 193 and 248 nm and 65% at 308 and 351 nm.

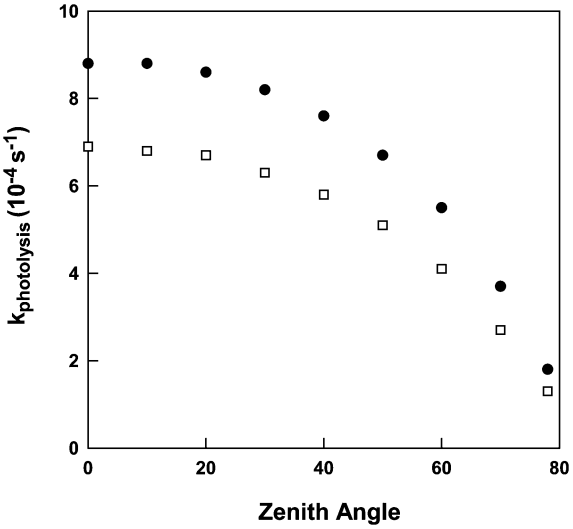

Figure 8. Atmospheric photolysis rate constants of *cis*-4-oxo-2-pentenal (circles) and *trans*-4-oxo-2-pentenal (squares) as a function of zenith angle.

pentenal determined in this work, and $\varphi(\lambda)$ represents the photolysis quantum yield for 4-oxo-2-pentenal. We used $J(\lambda)\Delta\lambda$ values reported by Demerjian et al.[29] In the photolysis rate calculation, $\varphi(\lambda)$ was assumed to be unity in the actinic UV region. The estimated photolysis rate constant will be lower if the photolysis quantum yield is less than the assumed quantum yield of unity at the longer wavelengths. The photolysis rate constants for 4-oxo-2-pentenal were estimated as a function of the zenith angle under cloudless conditions, at sea level, and for best-estimate albedo[30] (5% in the 290−400 nm region, 6% in the 400−450 nm region, 8% in the 450−460 nm region); the results are shown in Figure 8. Our estimated photolysis rate constants for *cis*-4-oxo-2-pentenal for zenith angles in the 0−60° range are 8.8×10^{-4} to 5.5×10^{-4} s^{-1}; these values correspond to photolysis lifetimes of 0.32 to 0.51 h. An upper limit for the photolysis loss of *cis*-4-oxo-2-pentenal in a smog chamber (1.6×10^{-3} s^{-1}) was previously given by Thüner et al.,[31] who dissolved a 4-oxo-2-pentenal sample in 1.0 mL of acetonitrile, sprayed the resulting solution into the chamber, and assumed that photolysis was the only loss process for 4-oxo-2-pentenal in the chamber. Our estimated photolysis rate constants for *trans*-4-oxo-2-pentenal for zenith angles in the 0−60° range are 6.9×10^{-4} to 4.1×10^{-4} s^{-1}; these values correspond to photolysis lifetimes of 0.40 to 0.68 h. Rate constants for 4-oxo-2-pentenal reactions with OH and O_3 have been reported[9,10] to be 5.6×10^{-11} and 4.8×10^{-18} $cm^3 molecule^{-1} s^{-1}$, respectively. With a 12-h average OH concentration[32,33] of 1.6×10^6 molecule/cm^3, and a 24-h average O_3 concentration[34] of 7×10^{11} molecule/cm^3, the 4-oxo-2-pentenal reaction lifetimes with OH and O_3 are 3.1 h and 3.4 days, respectively. Thus, photolysis is the dominant process for removal of 4-oxo-2-pentenal from the atmosphere.

Acknowledgment. We thank Di Hu for encouraging us to expand the scope of 4-oxo-2-pentenal photolysis study, so that the results can be directly incorporated into atmospheric chemistry models that simulate photochemical oxidation of aromatic compounds. Discussions with Dr. Ronghua Jin and Mr. Rui Zheng about 4-oxo-2-pentenal synthesis and with Drs. Katherine Alben, Oliver Rattigan, and Chris Judd are acknowledged. We thank Dr. Adriana Verschoor for critical readings of the manuscript and Lynn McNaughton at the Core NMR Facility of the Wadsworth Center for performing H NMR characterization of the 4-oxo-2-pentenal samples. We are grateful for the support provided by the National Science Foundation under grant No. ATM-0300294.

References and Notes

(1) Becker, K. H.; Barnes, I.; Bierbach, A.; Kirchner, F.; Thomas, W.; Wiesen, E.; Zabel, F. In *EUROTRAC Annual Reports*, Part 8; LACTOZ, Commission of the European Communities: Brussels, Belgium, 1991 and 1992.
(2) Barnes, I.; Becker, K. H.; Bierbach, A.; Wiesen, E. In *Laboratory Studies on Atmospheric Chemistry*; Air Pollution Research Report 42; Commission of the European Communities: Brussels, Belgium, 1991.
(3) Yu, J.; Jeffries, H. E.; Sexton, K. G. *Atmos. Environ*. **1997**, *31*, 2261.
(4) Smith, D. F.; McIver, C. D.; Kleindienst, T. E. *J. Atmos. Chem*. **1998**, *30*, 209.
(5) Smith, D. F.; Kleindienst, T. E.; McIver, C. D. *J. Atmos. Chem*. **1999**, *34*, 339.
(6) Bierbach, A.; Barnes, I.; Becker, K. H. *Atmos. Environ*. **1995**, *29*, 2651.
(7) Zhao, J.; Zhang, R. Y.; Misawa, K.; Shibuya, K. *J. Photochem. Photobiol., A* **2005**, *176*, 199.
(8) Hamilton, J. F.; Lewis, A. C.; Bloss, C.; Wagner, V.; Henderson, A. P.; Golding, B. T.; Wirtz, K.; Martin-Reviejo, M.; Pilling, M. J. *Atmos. Chem., Phys*. **2003**, *3*, 1999.
(9) Bierbach, A.; Barnes, I.; Becker, K. H.; Wiesen, E. *Environ. Sci. Technol*. **1994**, *28*, 715.
(10) Liu, X. Y.; Jeffries, H. E.; Sexton, K. G. *Environ. Sci. Technol*. **1999**, *33*, 4212.
(11) Liu, X. Atmospheric Photochemistry Study of 1,4-Unsaturated Dicarbonyls and Dienes, Ph.D. Thesis, University of North Carolina−Chapel Hill, Chapel Hill, NC, 1999.
(12) Di Hu, personal communication, University of North Carolina at Chapel Hill, 2005.
(13) O'Keefe, A.; Deacon, D. A. G. *Rev. Sci. Instrum*. **1988**, *59*, 2544.
(14) O'Keefe, A.; Scherer, J. J.; Cooksy, A. L.; Sheeks, R.; Health, J.; Saykally, R. J. *Chem. Phys. Lett*. **1990**, *172*, 214.
(15) Cronin, T. J.; Zhu, L. *J. Phys. Chem. A* **1998**, *102*, 10274.
(16) Tang, Y.; Zhu, L. *J. Phys. Chem. A* **2004**, *108*, 8307.
(17) Zhu, L.; Johnston, G. *J. Phys. Chem*. **1995**, *99*, 15114.
(18) Xu, G.; Liu, Y.; Sayre, L. M. *J. Org. Chem*. **1999**, *64*, 5732.
(19) Atkinson, R.; Baulch, D. L.; Cox, R. A.; Hampson, R. F., Jr.; Kerr, J. A.; Rossi, M. J.; Troe, J. *J. Phys. Chem. Ref. Data* **1997**, *26*, 521.
(20) Meller, R.; Raber, W.; Crowley, J. N.; Jenkin, M. E.; Moortgat, G. K. *J. Photochem. Photobiol., A* **1991**, *62*, 163.
(21) Staffelbach, T. A.; Orlando, J. J.; Tyndall, G. S.; Calvert, J. G. *J. Geophys. Res*. **1995**, *100*, 14189.
(22) Chen, Y.; Wang, W.; Zhu, L. *J. Phys. Chem. A* **2000**, *104*, 11126.
(23) O'Connor, M. P.; Wenger, J. C.; Mellouki, A.; Wirtz, K.; Munoz, A. *Phys. Chem. Chem. Phys*. **2006**, *8*, 5236.
(24) Tang, Y.; Zhu, L. *Chem. Phys. Lett*. **2005**, *409*, 151.
(25) Stoeckel, F.; Schuh, M. D.; Goldstein, N.; Atkinson, G. H. *Chem. Phys*. **1985**, *95*, 135.
(26) Zhong, Q.; Steinhurst, D. A.; Baronavski, A. P.; Qwrutsky, J. C. *Chem. Phys. Lett*. **2003**, *370*, 609.
(27) Owrutsky, J. C.; Baronavski, A. P. *J. Chem. Phys*. **1998**, *108*, 6652.
(28) Zhong, Q.; Poth, L.; Castleman, A. W. *J. Chem. Phys*. **1999**, *110*, 192.
(29) Demerjian, K. L.; Schere, K. L.; Peterson, J. T. *Adv. Environ. Sci. Technol*. **1980**, *10*, 369.
(30) Coulson, K. L.; Reynolds, D. W. *J. Appl. Meteorol*. **1971**, *10*, 1285.
(31) Thüner, L. P.; Rea, G.; Wenger, J. In *The European Photoreactor EUPHORE 4th Report 2001*; Barnes, I., Ed.; Valencia, Spain, February 2004; pp 47−53.
(32) Prinn, R.; Cunnold, D.; Simmonds, P.; Alyea, F.; Boldi, R.; Crawford, A.; Fraser, P.; Gutzler, D.; Hartley, D.; Rosen, R.; Rasmussen, R. *J. Geophys. Res*. **1992**, *97*, 2445.
(33) Crutzen, P. J.; Zimmermann, P. H. *Tellus* **1991**, *43AB*, 136.
(34) Logan, J. A. *J. Geophys. Res*. **1985**, *90*, 10463.